

## A NUMERICAL ENDEAVOR WITH NONLINEAR KAWARADA EQUATIONS

QIN SHENG<sup>†,1</sup> AND YONGBIN GE<sup>‡,2</sup>

<sup>†</sup>Department of Mathematics and Center for Astrophysics Space Physics and Engineering Research, Baylor University, Waco, TX 76798-7328, USA

<sup>‡</sup>School of Mathematics and Computer Science, Ningxia University, Yinchuan, Ningxia 750021, China

**ABSTRACT.** This exploration concerns the numerical solution of degenerate singular reaction-diffusion equations. The nonlinear partial differential equations are introduced by H. Kawarada, and studied and analyzed extensively by Professor C. Y. Chan and collaborators. Remarkable theory and applications are accomplished. Based on these, this paper revisits and reevaluates some of the most fascinating properties of Kawarada equation solutions through advanced numerical computations. The significance of the latest numerical methods constructed for solving these legendary nonlinear singular problems are also reassessed.

**Keywords.** Kawarada equations, quenching singularity, degeneracy, Crank-Nicolson method, grid adaptations, stability, monotonicity

**AMS (MOS) Subject Classification.** 65M06, 65M12, 65M50, 65Z05, 35K20

*This paper is dedicated to Professor C. Y. Chan for his contributions in applied and computational mathematics*

### 1. Introduction

Consider the following nonlinear Kawarada equation together with homogeneous Dirichlet boundary conditions and an initial condition,

$$(1.1) \quad \sigma(x) \frac{\partial u}{\partial t} = \sum_{k=1}^n \frac{\partial^2 u}{\partial x_k^2} + f(u), \quad x \in \Omega, \quad t > t_0,$$

$$(1.2) \quad u(x, t) = 0, \quad x \in \partial\Omega, \quad t > t_0,$$

$$(1.3) \quad u(x, t_0) = u_0(x), \quad x \in \Omega,$$

---

<sup>1</sup>Corresponding author. Email address: Qin\_Sheng@baylor.edu .

<sup>2</sup>The second author is supported in part by a research grant, No. 11361045, from the National Science Foundation of China, China.

where  $\Omega \subset \mathbb{R}^n$  and  $\partial\Omega$  is the boundary of  $\Omega$ ,  $0 \leq u_0 \ll 1$ , and

$$f(0) = f_0 > 0, \quad f_u(u) > 0, \quad \lim_{u \rightarrow 1^-} f(u) = \infty.$$

The nonnegative degeneracy function  $\sigma(x)$  diminishes to zero only for  $x \in \Omega_0 \subset \partial\Omega$  [1–10, 15, 16, 18–22].

It is known that the solution of (1.1)–(1.3) increases monotonically till the unity is reached at any spatial position as time  $t$  increases. Further, it is predicted that if the shape of  $\Omega$  is fixed, then there exists a critical number  $a^* > 0$  such that if  $a$ , the  $n$ -volume of  $\Omega$ , is less than  $a^*$  then the solution of (1.1)–(1.3) exists globally. Otherwise there exists a finite time  $T^*(a)$  such that

$$\lim_{t \rightarrow T^*(a)} \sup_{x \in \Omega} u(x, t) = 1.$$

Such an  $a^*$  is called a *critical value* and  $T^*$  a *critical time* [6–8, 15]. The function  $u$  is referred as a *quenching solution* in the latter case. A particularly interesting example of the quenching is the one-dimensional case of (1.1)–(1.3) when  $\sigma \equiv 1$  and

$$(1.4) \quad f(u) = \frac{1}{1-u}.$$

In the circumstance the critical value, that, the critical spatial interval length, is  $a^* \approx 1.53045607591062$  [5, 17, 21]. Numerous recent computations have also devoted to verify this fascinating property [1–3, 10, 13, 17–25].

Our discussion is organized as follows. In the next section, we provide a modern numerical framework for the solution of degenerate one-dimensional Kawarada equation problem Ra01–(1.3). A generalized Crank-Nicolson type approximation is adopted. Uniform and nonuniform meshes are considered for both space and time. Mesh moving adaptations are controlled via properly designed arc-length monitoring functions [16, 18]. Key numerical analysis results on the numerical stability, solution monotonicity and convergence are given. In Section 3, two computational experiments are carried out to validate and demonstrate quenching and no quenching solutions via the latest adaptive and semi-adaptive algorithms constructed. Important limiting values that lead to the occurrence of quenching are evaluated carefully with the particular degeneracy and source functions. Brief concluding remarks and discussions are given for continuing studies in the last Section.

## 2. Degenerate Kawarada problems

We are particularly interested in the circumstance in which  $n = 1$ ,  $\sigma(x) = ax^p(1-x)^{1-p}$ , and  $f(u) = 1/(1-u)^q$ ,  $0 \leq p \leq 1$ ,  $q > 0$ , due to its recent applications in rocket fuel combustion modeling and simulations [9, 11, 23]. For the sake of simplicity,

we may map the general spatial interval  $[0, a]$  to  $[0, 1]$ . Thus, (1.1)–(1.3) can be reformulated to the following:

$$(2.1) \quad \sigma(x) \frac{\partial u}{\partial t} = \frac{1}{a^2} \frac{\partial^2 u}{\partial x^2} + \frac{1}{(1-u)^q}, \quad 0 < x < 1, \quad t_0 < t \leq T,$$

$$(2.2) \quad u(0, t) = u(1, t) = 0, \quad t_0 < t \leq T,$$

$$(2.3) \quad u(x, t_0) = u_0(x), \quad 0 < x < 1,$$

where  $T > 0$  is sufficiently large.

We note that the following limits are equivalent [7, 9, 21],

$$\lim_{t \rightarrow T^*(a)} \sup_{0 < x < 1} u(x, t) = 1, \quad \lim_{t \rightarrow T^*(a)} \sup_{0 < x < 1} u_t(x, t) = +\infty \text{ whenever } a > a^*.$$

We further rewrite the dimensionless model (2.1)–(2.3) as the standard Kawarada problem:

$$(2.4) \quad \frac{\partial u}{\partial t} = \phi(x) \frac{\partial^2 u}{\partial x^2} + \psi(x, u), \quad 0 < x < 1, \quad t_0 < t \leq T,$$

$$(2.5) \quad u(0, t) = u(1, t) = 0, \quad t_0 < t \leq T,$$

$$(2.6) \quad u(x, t_0) = u_0(x), \quad 0 < x < 1,$$

where

$$(2.7) \quad \phi(x) = \frac{1}{a^2 \sigma(x)}, \quad \psi(x, u) = \frac{1}{\sigma(x)(1-u)^q}.$$

Let  $N \gg 1$  and  $\bar{\mathcal{D}}_N = \{x_0, x_1, \dots, x_{N+1}\}$  be an arbitrary spatial mesh superimposing  $[0, 1]$ . For it we set  $0 < x_{k+1} - x_k = h_k \ll 1$ ,  $k = 0, 1, \dots, N$ , to be variable step sizes. We often require the following smoothness constraint [11],

$$0 < m \leq \frac{h_k}{h_{k+1}} \leq M \ll \infty, \quad k = 0, 1, 2, \dots, N - 1,$$

for given constants  $m$  and  $M$ . Assume that  $\mathcal{D}_N \subset \bar{\mathcal{D}}_N$  be the set of interior mesh points. We approximate the spatial derivative at  $x_k \in \mathcal{D}_N$  by the central difference,

$$\frac{\partial^2 u}{\partial x^2}(x_k, t) = \frac{h_k u_{k-1}(t) - (h_{k-1} + h_k) u_k(t) + h_{k-1} u_{k+1}(t)}{h_{k-1} h_k^2} + \mathcal{O}(h),$$

where  $h = \max_{k=0,1,\dots,N} h_k$ . In the case if  $\mathcal{D}_N$  is uniform, the above provides a standard second-order central difference formula, that is,

$$\frac{\partial^2 u}{\partial x^2}(x_k, t) = \frac{u_{k-1}(t) - 2u_k(t) + u_{k+1}(t)}{h^2} + \mathcal{O}(h^2), \quad h = \frac{1}{N+1}.$$

Thus, the following initial value problem follows immediately from (2.4)–(2.7),

$$(2.8) \quad \frac{du}{dt} = Au + \psi, \quad t > t_0,$$

$$(2.9) \quad u(t_0) = u_0,$$

where  $u = (u_1, u_2, \dots, u_N)^\top$ ,  $\psi = (\psi_1, \psi_2, \dots, \psi_N)^\top$ . We have  $A = BT \in \mathbb{R}^{N \times N}$  with  $B = \text{diag}[\phi_1, \phi_2, \dots, \phi_N]$ ,  $\phi_k > 0$ ,  $k = 1, 2, \dots, N$ , and  $T$  is tridiagonal. However,  $T$  is not TST unless a uniform spatial mesh is used [2]. The solution of (2.8), (2.9) exists and is unique if  $Au + \psi$  satisfies the Lipschitz condition [12, 15]. A formal solution of the system can thus be formulated as

$$(2.10) \quad u(t) = E(tA)u_0 + \int_{t_0}^t E((t-\tau)A)\psi(u(\tau))d\tau, \quad t \geq t_0,$$

where  $E(\cdot) = \exp(\cdot)$  is the matrix exponential. It can be shown that all eigenvalues of  $A$  are real and negative. Further, for the matrix exponential  $E(tA)$ ,

$$(2.11) \quad E(tA) = B^{1/2}E(tB^{1/2}TB^{1/2})B^{-1/2},$$

where  $t \in \mathbb{C}$ . Thus, if  $t \in \mathbb{R}^+$  then all eigenvalues of  $E(tA)$  are real and  $\rho(tA) < 1$ , where  $\rho(\cdot)$  is the spectral radius of the matrix.

An application of the trapezoidal rule to (2.10) yields

$$u(t) \approx E((t-\tau_0)A)u_0 + \frac{t-t_0}{2} [\psi(u(t)) + E((t-t_0)A)\psi(u_0)], \quad t \geq t_0.$$

Further, if we consider an  $A$ -acceptable [2/2] Padé approximant,

$$E(tA) \approx \left(I - \frac{t}{2}A\right)^{-1} \left(I + \frac{t}{2}A\right),$$

then we arrive at an adaptive Crank-Nicolson type finite difference platform for solving (2.4)–(2.6),

$$(2.12) \quad u^{(j+1)} = \left(I - \frac{\tau_j}{2}A\right)^{-1} \left(I + \frac{\tau_j}{2}A\right) \left[u^{(j)} + \frac{\tau_j}{2}\psi(u^{(j)})\right] + \frac{\tau_j}{2}\psi(u^{(j+1)}),$$

$$(2.13) \quad u^{(0)} = u_0,$$

where variable steps  $\tau_j$ ,  $h_k$  can be determined through different monitoring functions [17]. Needless to mention, an iterative procedure, or an approximation of the last term in (2.12), needs to be utilized for completing the nonlinear system solution procedure. Since the high nonlinearity of  $\psi$  often leads to multiple solutions of (2.12), (2.13) and upper-lower vectors can be incorporated (see [18] and references therein), the latter choice becomes more favorable to our next step computations.

We may state

**Theorem 2.1.** *If the nonlinear function  $\psi$  is frozen, then the Crank-Nicolson type platform (2.12), (2.13) is unconditionally linearly stable.*

**Theorem 2.2.** *Suppose that the last term in (2.12) is approximated precisely during the computation. Then for any initial numerical error  $\epsilon^{(j)}$  and any nonnegative integers  $m, j$ , an upper bound of the error growth due to (2.12), (2.13) is*

$$\|\epsilon^{(j+m+1)}\|_2 < K_{j,m} \sqrt{\text{cond}(B^{1/2})} \|\epsilon^{(j)}\|_2, \quad m, j \in \{0, 1, 2, \dots\},$$

where

$$K_{j,m} = \prod_{\ell=j}^{m+j} \max_{k=1,\dots,N} d_k^{(\ell)} \max_{s=1,\dots,N} \sqrt{d_s^{(j+m+1)}},$$

$$d_k^{(\ell)} = 1 + \frac{q\tau_\ell}{2 \left(1 - \xi_k^{(\ell)}\right)^{q+1} \sigma(x_k)}, \quad 0 < \xi_k^{(\ell)} < 1.$$

**Theorem 2.3.** *For any beginning solution  $u^{(\ell)} < 1$ ,  $\ell \geq 1$ , if*

- (i)  $\gamma_j = \tau_j/h^2 \leq a^2\phi_{\min}$ ;
- (ii)  $d_k^{(j)} \leq 2$ ,  $k = 1, 2, \dots, N$ ;
- (iii)  $Au^{(j)} + \psi(u^{(j)}) \geq 0$ ,

where  $j = \ell, \ell + 1, \ell + 2, \dots$ , then the solution vector sequence  $u^{(\ell)}, u^{(\ell+1)}, u^{(\ell+2)}, \dots$ , produced by the adaptive, or semi-adaptive, scheme (2.12), (2.13) increases monotonically until unity is exceeded by a component of the vector (that is, until quenching occurs) or converges to the steady solution of the problem. In the latter case, we do not have a quenching solution.

We note that condition (iii) of Theorem 2.3 has been ensured at least for the case  $\ell = 0$  and  $u^{(0)}$ . It seems that the solution monotonicity requires more rigorous constraints than those for the numerical stability and convergence. This additional numerical feature is definitely justified for ensuring expected quenching phenomena. However, the monotonicity requirement has also made applications of nonuniform spacial grids extremely challenging.

### 3. Numerical endeavors

Our experiments have again validated results presented in [1, 3, 20–23] where similar differential equation structures are entertained. Since computational procedures carried out are similar, there is little need to repeat most standard data, figures and simulations. Instead, we only show key illustrations of solutions of the singular reaction-diffusion equation with new and different degenerate functions in Section 1. To this end, we consider (2.4)–(2.6) with  $0 \leq p \leq 1$  and  $q > 0$ .

Without loss the generality, in following discussions, unless specially declared, we may set  $q = 1$  and let the temporal adaptation start once  $v(t) = \max_{0 \leq x \leq 1} u(x, t)$  reaches a certain criterion, say,  $v^* = 0.95$ . For different values of  $a$ , possible corresponding quenching time and locations are searched and confirmed if they do exist. Our second-order semi-adaptive, or the first-order adaptive, algorithm (2.12), (2.13) is found to be extremely easy and reliable to use. The variable  $t$ -step and  $x$ -step generators are effective and accurate. CFL numbers [12] used for the stability of the adaptive implicit schemes are around the unity. All computations are either implemented

using FORTRAN 95 with desirable NAG subroutines or parallel MATLAB-SIMULINK packages on cluster computers.

For the purpose of simplicity in programming, we may reorganize (2.12) to

$$\left(I - \frac{\tau_j}{2}A\right) u^{(j+1)} = \left(I + \frac{\tau_j}{2}A\right) u^{(j)} + g(u^{(j)}, w^{(j+1)}), \quad j = 0, 1, \dots,$$

where

$$g(u^{(j)}, w^{(j+1)}) = \frac{\tau_j}{2} \left[ \left(I + \frac{\tau_j}{2}A\right) \psi(u^{(j)}) + \left(I - \frac{\tau_j}{2}A\right) \psi(w^{(j+1)}) \right],$$

and  $w^{(j+1)}$  is determined through a forward Euler scheme. We consider homogeneous Dirichlet boundary conditions and following a smooth initial data stream,

$$u_0(x) = \mu \sin \frac{\pi x}{a}, \quad 0 \leq x \leq a, \quad 0 \leq \mu \ll 1.$$

Case I (no quenching). Take  $a = 1, \mu = 0.001, 0.005$ .

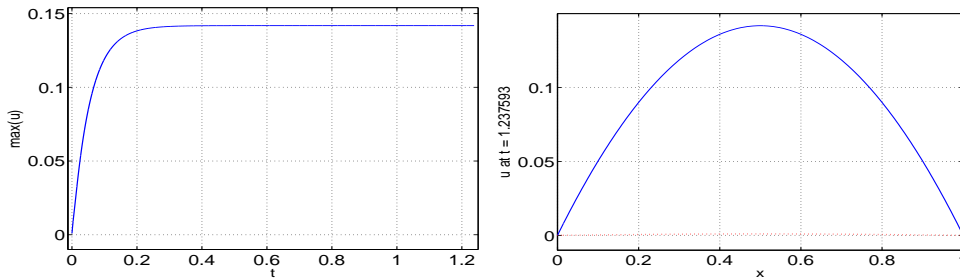


FIGURE 3.1. Profiles of the maximal values of the solution  $u$ . LEFT:  $\max_x u$  profile as  $t$  increases. RIGHT:  $u$  at the end of experiments with the initial function plotted in red as a comparison. Over 200,000 temporal steps are executed. Adaptation has never been activated due to flat  $u_t$  values. No quenching solution is observed.

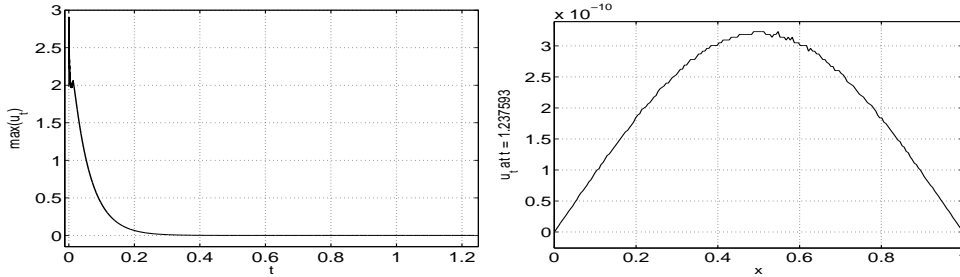


FIGURE 3.2. Profiles of the maximal values of the rate of change function  $u_t$ . LEFT:  $\max_x u_t$  profile as  $t$  increases. RIGHT: the derivative  $u_t$  at the end of experiments. Up to 200,000 temporal steps are executed. Adaptation has never been activated due to flat  $u_t$  values. Again, no quenching solution is observed.

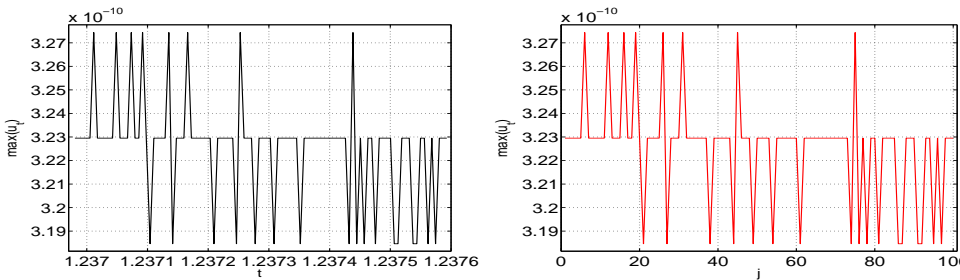


FIGURE 3.3. Profiles of the maximal values of the rate of change function  $u_t$ . LEFT:  $\max_x u_t$  profile with respect to the  $t$  values. RIGHT:  $\max_x u_t$  profile with respect to the  $t$  values. Adaptation has never been triggered due to the relatively smooth  $u_t$  values.

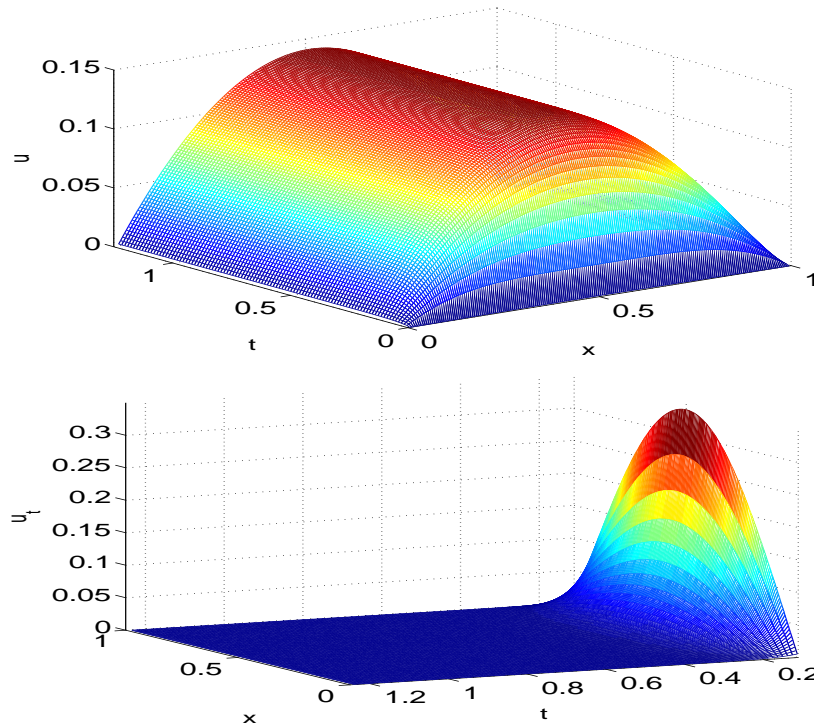


FIGURE 3.4. Three-dimensional views of  $u$  and  $u_t$ . TOP: Plot of  $u$  ranging for  $t \in [0, 1.2376]$ . BOTTOM: Plot of  $u$  ranging for  $t \in [0.1, 1.2376]$ .

It can be observed in Figures 3.1 and 3.2 that, while the solution  $u$  increases monotonically, the rate of change function  $u_t$  decreases continuously as  $t$  increases. As a consequence,  $u$  becomes extremely smooth and flat. Its maximal values seemly take  $u^* \approx 0.141830 \ll 1$  as a possible ceiling.

We show maximal values of the final 100 rate of change functions  $u_t$  for (2.4)–(2.6) in Figure 3.3. We note that, though the values changes due to computational errors, the rate function remains being positive, which is a strong evidence of the monotonicity of the solution  $u$ .

Although the degeneracy plays a significant role of disturbances during the initial stage of computations, the strong diffusion dominates in later stages of computations. We show these features more clearly in Figures 3.4, where 3D views of the  $u$ ,  $u_t$  are given. Figures with different values of  $\mu$  are similar. The phenomena demonstrated fit consistently with theoretical predictions given by C. Y. Chan et. al [5, 7, 10, 14].

Case II (quenching). Take  $a = \pi$  and  $\mu = 0.001$ .

Let us first present profiles of  $u$  and  $u_t$  in Figures 3.5–6. Different from the previous situation, a strong quenching singularity occurs in the current situation. It is found that as soon as the time  $t$  approaches  $T_\pi^* \approx 0.792907811312324$ ,  $u$  quenches and  $u_t$  blows up simultaneously. The adaptation is activated at  $\max_x u = 0.95$  and

remains for the rest of journey of computations. To see more precisely characteristic structures and features of the solutions, in Figure 3.7–9, we show 3D surfaces of both  $u$  and  $u_t$ . The first pair is taken for the entire evolution process. The second pair is for those on final 50 time steps before quenching, and Figure 3.9 is devoted to the solution and rate of change function in the first 120 temporal steps in the journey. It is observed that while  $u$  approaches the unity in the center of the spacial domain smoothly in this case,  $u_t$  blows up violently at the quenching time  $T_\pi^*$ . The interesting phenomena are again consistently with theoretic predictions and our previous investigations [6, 8, 19, 20, 22].

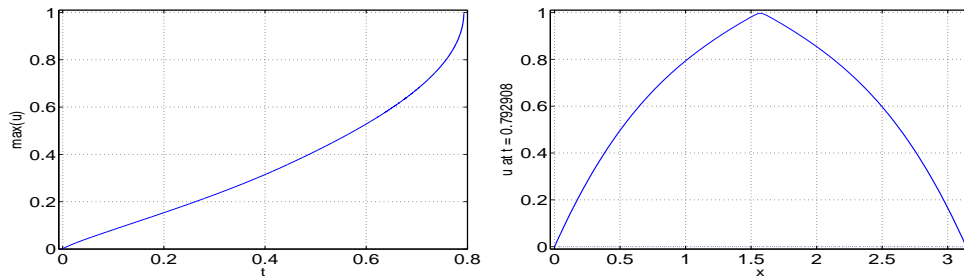


FIGURE 3.5. Profiles of solution  $u$ .  $p = 0.5$  is used. LEFT:  $\max_x u$  increases. RIGHT:  $u$  immediately before the quenching. Up to 12,983 temporal steps are used. Temporal adaptation kicks in at  $\max_x u \approx 0.95$  and remains on throughout the rest of calculations. Quenching solution is observed with a quenching time  $T_\pi^* \approx 0.792907811312324$ .

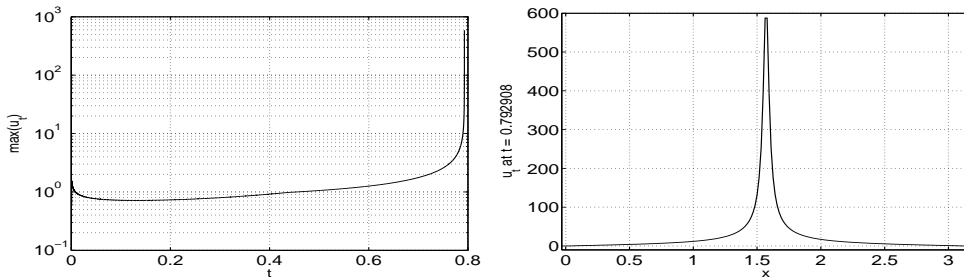


FIGURE 3.6. Profiles of the rate of change function  $u_t$ .  $p = 0.5$  is used. LEFT:  $\max_x u_t$  as  $t$  increases. A logarithmic  $y$ -scale is utilized. RIGHT:  $u_t$  immediately before the quenching. Up to 12,983 temporal steps are executed. Again, quenching solution is observed with a quenching time  $T_\pi^* \approx 0.792907811312324$ .

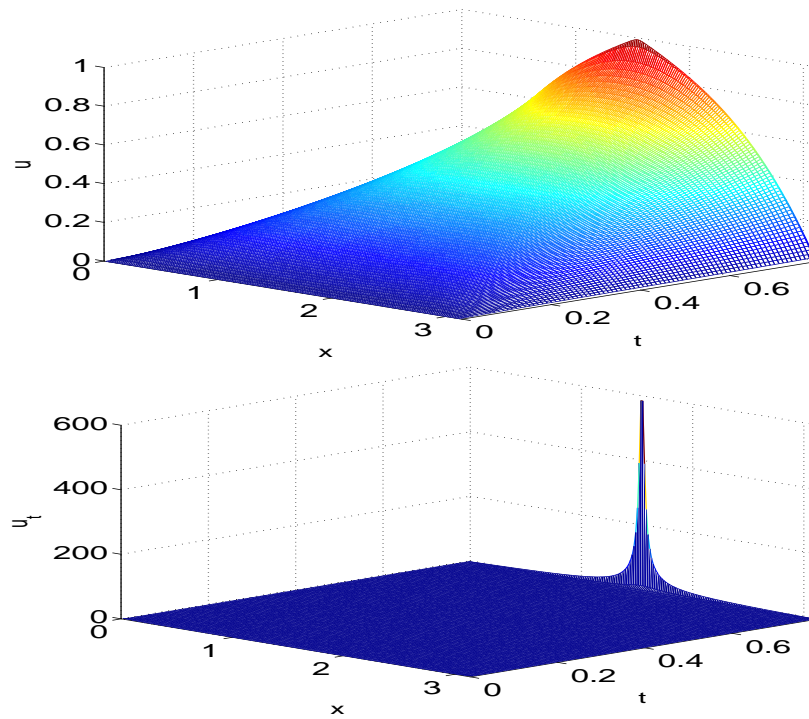


FIGURE 3.7. Three-dimensional views of  $u$  and  $u_t$  till the quenching ( $0 \leq t \leq 0.792907$ ). Peak value of  $u_t \approx 587.781919$  is reached. Quenching is observed.

More details of the numerical solutions near quenching are provided by Figure 3.8.

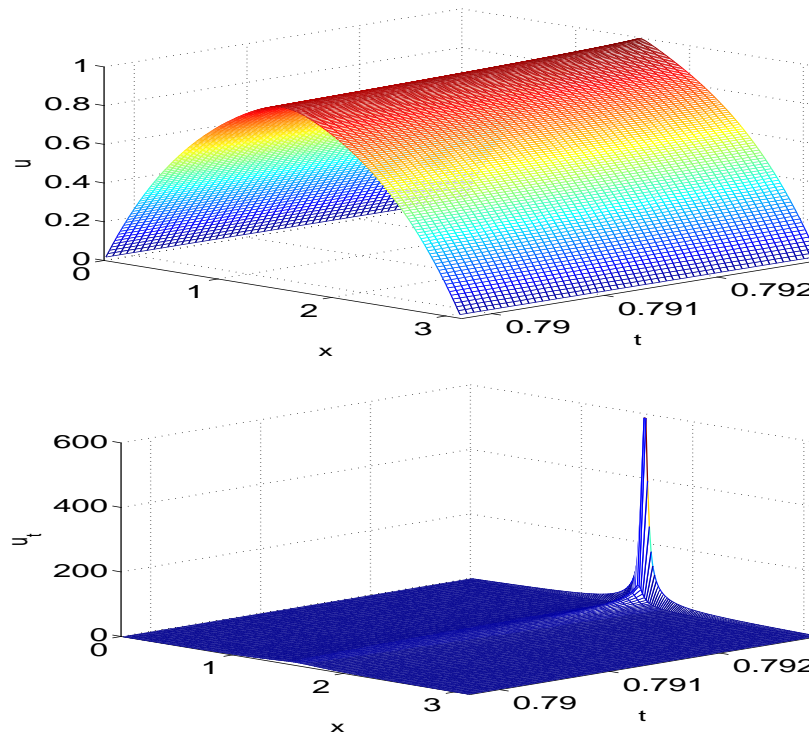


FIGURE 3.8. Three-dimensional views of  $u$  and  $u_t$  in the last 50 temporal steps ( $0.789732027118516 \leq t \leq 0.792907811312324$ ). Peak value of  $u_t \approx 587.781919$ . The blow-up rate of  $u_t$  is clearly significant.

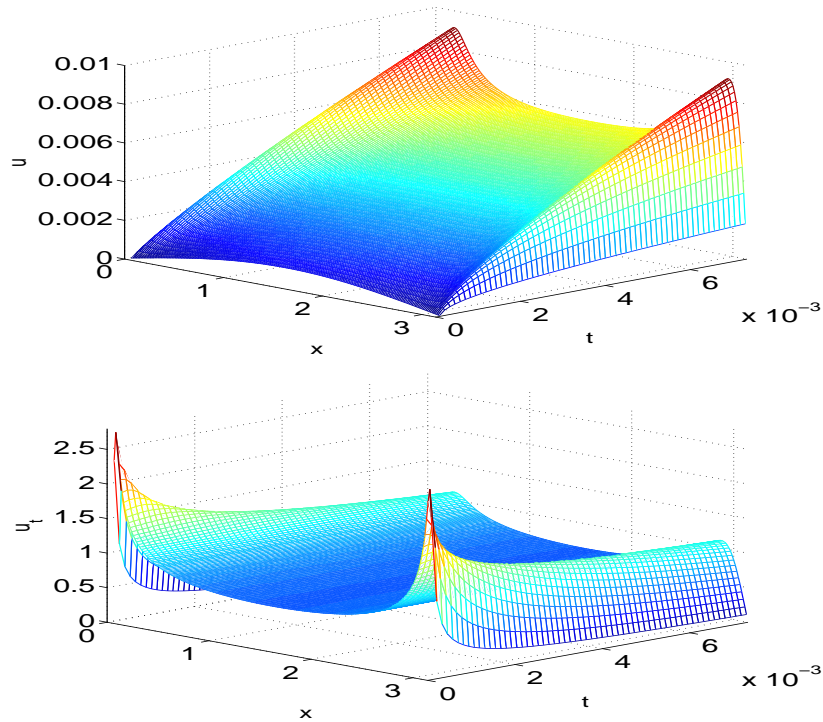


FIGURE 3.9. Three-dimensional views of  $u$  and  $u_t$  in the first 120 temporal steps ( $0 \leq t \leq 0.007329$ ). Peak value of  $u_t \approx 2.741833$ . The degenerate singularity near the end points is visible.

Apparently, the impact of the degeneracy is continuously to be true in this case. To view this, we have more details of solutions in Figure 3.9, where  $p = 0.5$  is utilized. The initial 120 temporal steps are displayed. It can be seen that contributions of the degeneracy near both ends of the spacial interval are significant. Further, we use different value of  $p = 0.66$  in Figure 3.10. Firstly, solutions of (2.4)–(2.6) in initial 2,000 temporal steps are computed. It has been seen again that contributions of the degeneracy near ends of the spacial interval are significant. We may observe that, probably due to the strong diffusion features of the differential equation and numerical stability of the full adaptive/semi-adaptive methods (2.12), (2.13), disturbances of degeneracy at endpoints diminish as the solution advances. Thirdly, we have found that the degeneracy does affect the solution symmetry. In the last row of figures, numerical solutions are apparently pushed toward  $x = 0$  by the stronger degeneracy at  $x = 0$ . As a consequence, the quenching location is slightly shifted to  $x^* \approx 1.219125507363203$ . In this position, the rate of change function  $u_t$  teaches its peak value 968.5546875500277.

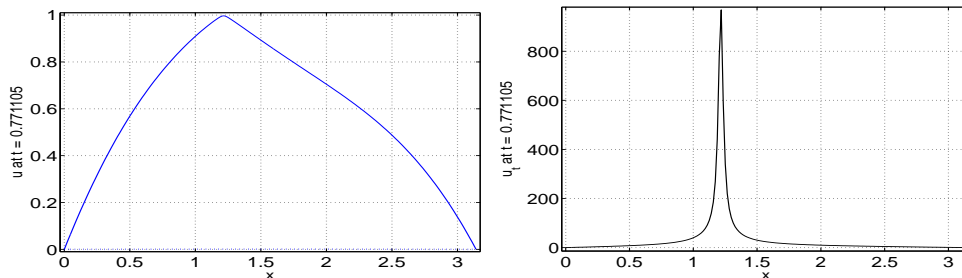


FIGURE 3.10. Profiles of solution  $u$  (blue) and  $u_t$  (black) with  $a = \pi$ ,  $p = 0.66$  and  $\mu = 0.01$ . LEFT:  $u$  immediately before the quenching. RIGHT:  $u_t$  immediately before the quenching near the end of experiments. Up to 12,626 temporal steps are executed. Adaptation kicks in once  $\max_x u \geq 0.95$ . Quenching solution is observed with a quenching time  $T_\pi^* \approx 0.771104831366368$  and quenching location  $x^* \approx 1.219125507363203$  for the maximum of  $u_t \approx 968.5546875500277$ .

To see more about the influence of degeneracy on quenching singularity, here-with we show the numerical solution  $u$  immediately before quenching in Figure 3.11. Different  $p$  values are employed. Detailed information about the quenching time and location is given in Table 3.1. It is interesting to notice that neither the quenching location  $x^*$  nor the quenching time  $T^*$  is a simple linear function of  $p$ .

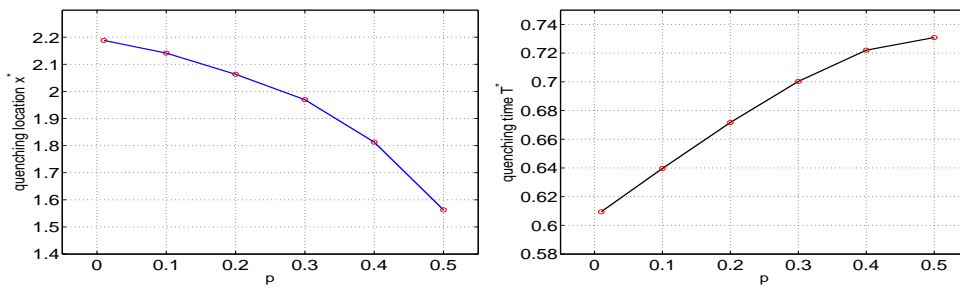


FIGURE 3.11. Relations of the quenching time  $T_\pi^*$  and location  $x_\pi^*$  when different  $p$  values are used in the degeneracy function. It is observed while the  $p$  value increases, the quenching time increases and quenching location decreases for  $p \in (0, 0.5]$ . Neither the quenching location  $x^*$  nor the quenching time  $T^*$  is a simple linear function of  $p$ . Kawarada problem (2.4)–(2.6) is utilized.

$p$	$T_\pi^*$	$x_\pi^*$
0.01	0.609506274119872	2.188173987574980
0.1	0.639615151188096	2.141284544984088
0.2	0.671678356990973	2.063135473999267
0.3	0.700321487508209	1.969356588817482
0.4	0.722063394681207	1.813058446847841
0.5	0.730884483378537	1.562981419696415

TABLE 3.1. Quenching time  $T_\pi^*$  and location  $x_\pi^*$  when different  $p$  values are used in the degeneracy function. Parameters used are the same as in Figure 3.11. It is observed while the  $p$  value increases, the quenching time increases and quenching location decreases for  $p \in (0, 0.5]$ .

An optimized artificial singularity remover [17] is used to secure the source function during computations. It is anticipated that values of  $u$  to decline once the source function becomes negative. This is clearly observed in our numerical experiments. The observation also links to a more sensitive issue of research in post-quenching, that is, after quenching, mechanism [4, 15, 17, 21]. More rigorous numerical study is definitely required for this type of investigations.

#### 4. Conclusions

To conclude, in this paper, we have reviewed and restudied some latest adaptive, semi-adaptive finite difference methods for solving a degenerate Kawarada equation problem. The one-dimensional nonlinear model equation is closely related to multi-physical applications, in particular in quenching-combustion and rocket fuel burning controls [5, 23]. New study and improved analysis of key characteristic issues, including the nonlinear stability, monotonicity, and conservations of the numerical scheme, are mentioned. Several simulation experiments are given not only for demonstrating singular numerical solutions, but also the degeneracy and across quenching point singularities. These have been basic properties of the Kawarada equations pointed out by C. ;Y. Chan and other investigators.

The numerical method studied utilizes uniform and nonuniform meshes in the space. Although adaptations in the space may reduce the overall accuracy of a finite difference method if the algorithmic simplicity needs to be preserved [13, 24], our forthcoming research will provide an optimized balance between the spacial adaptation and efficiency for solving multidimensional singular reaction-diffusion equations.

Yet many important and interesting computational issues related to singular problems such as (1.1)–(1.3), (2.1)–(2.3) and (2.4)–(2.6), including the use of nonlocal boundary conditions, coupled equations with distinctive singular features, nonlinear degeneracy impact to the quenching, and numerical impulsive quenching for highly effective fuel combustion designs, are still open. We would wish this simple article to serve as one of the ignition sparks to promote further researches in this extremely promising field.

**Acknowledgement:** The authors would like to thank the anonymous referees for their valuable comments and suggestions that have enhanced the quality and presentation of this paper.

#### REFERENCES

- [1] M. Beauregard and Q. Sheng, Solving degenerate quenching-combustion equations by an adaptive splitting method on evolving grids, *Computers Stru.*, 122:33–43, 2013.
- [2] M. Beauregard and Q. Sheng, An adaptive splitting approach for the quenching solution of reaction-diffusion equations over nonuniform grids, *J. Computat. Appl. Math.*, 241:30–44, 2013.
- [3] M. Beauregard and Q. Sheng, A fully adaptive approximation for quenching type reaction-diffusion equations over circular domains, *Numer. Meth. PDEs.*, 30:472–489, 2014.
- [4] C. Y. Chan and H. G. Kaper, Quenching for semilinear singular parabolic problems, *SIAM J. Math. Anal.*, 20:558–566, 1997.
- [5] C. Y. Chan and L. Ke, Parabolic quenching for nonsmooth convex domains, *J. Math. Anal. Appl.*, 186:52–65, 1994.
- [6] C. Y. Chan and P. C. Kong, Solution profiles beyond quenching for degenerate reaction-diffusion problems, *Nonlinear Analysis: Theory, Methods Appl.*, 24:1755–1763, 1995.

- [7] C. Y. Chan and P. Tragoonsirisak, A multi-dimensional quenching problem due to a concentrated nonlinear source in RN, *Nonlinear Analysis: Theory, Methods Appl.*, 69:1494–1514, 2008.
- [8] C. Y. Chan and J. Yang, Complete blow-up for degenerate semilinear parabolic equations, *J. Comput. Appl. Math.*, 113:353–364, 2000.
- [9] H. Cheng, P. Lin, Q. Sheng and R. C. E. Tan, Solving degenerate reaction-diffusion equations via variable step Peaceman-Rachford splitting, *SIAM J. Sci. Comput.*, 25:1273–1292, 2003.
- [10] P. Ferreira, Numerical quenching for the semilinear heat equation with a singular absorption, *J. Comput. Appl. Math.*, 228: 92–103, 2009.
- [11] R. M. Furzeland, J. G. Verwer and P. A. Zegeling, A numerical study of three moving-grid methods for one-dimensional partial differential equations which are based on the method of lines, *J. Comput. Phys.*, 89:349–388, 1990.
- [12] A. Iserles, *A First Course in the Numerical Analysis of Differential Equations*, Cambridge University Press, 2nd Ed., New York, 2011.
- [13] B. Jain and A. Sheng, An exploration of the approximation of derivative functions via finite differences, *Rose-Hulman Undergrad. Math J.*, 8:172–188, 2007.
- [14] H. Levine, Quenching, nonquenching, and beyond quenching for solutions of some parabolic equations, *Ann. Math. Pure Appl.*, 4:243–260, 1989.
- [15] N. Nouaili, A Liouville theorem for a heat equation and applications for quenching, *Nonlinearity*, 24:797–832, 2011.
- [16] Z. Qiao, Z. Zhang and T. Tang, An adaptive time-stepping strategy for the molecular beam epitaxy models, *SIAM J. Sci. Comput.*, 33:1395–1414, 2011.
- [17] Q. Sheng, Adaptive decomposition finite difference methods for solving singular problems, *Frontiers Math. China*, 4:599–626, 2009.
- [18] Q. Sheng and R. Agarwal, Nonlinear variation of parameter methods for summary difference equations in several independent variables, *J. Appl. Math. Comput.*, 61:39–60, 1994.
- [19] Q. Sheng and H. Cheng, An adaptive grid method for degenerate semilinear quenching problems, *Computers Math. Appl.*, 39:57–71, 2000.
- [20] Q. Sheng and A. Q. M. Khaliq, A compound adaptive approach to degenerate nonlinear quenching problems, *Numer. Meth. PDEs.*, 15:29–47, 1999.
- [21] Q. Sheng and A. Q. M. Khaliq, Linearly implicit adaptive schemes for singular reaction-diffusion equations, Chapter 9, *Adaptive Method of Lines*, CRC Press, London and New York, 2001.
- [22] Q. Sheng and A. Q. M. Khaliq, Modified arc-length adaptive algorithms for degenerate reaction-diffusion equations, *Appl. Math. Comput.*, 126:279–297, 2002.
- [23] Q. Sheng and A. Q. M. Khaliq, A revisit of the semi-adaptive method for singular degenerate reaction-diffusion equations, *East Asia J. Appl. Math.*, 2:185–203, 2012.
- [24] Z. J. Tan, Z. R. Zhang, Y. Q. Huang and T. Tang, Moving mesh methods with locally varying time steps, *J. Comput. Phys.*, 200:347–367, 2004.